AGU PUBLICATIONS

JGR

Journal of Geophysical Research: Atmospheres

RESEARCH ARTICLE
10.1002/2016JD025527

Key Points:
- Q_{si} estimates were found to have large biases when evaluated over a region of complex terrain
- Q_{si} errors were related to precipitation but not aerosols or water vapor
- Users of these estimates need to be aware of this large source of uncertainty in complex terrain

Supporting Information:
- Supporting Information S1

Correspondence to:
K. E. Lapo,
lapok@uw.edu

Citation:
Lapo, K. E., L. M. Hinkelman, E. Sumargo, M. Hughes, and J. D. Lundquist (2017), A critical evaluation of modeled solar irradiance over California for hydrologic and land surface modeling, *J. Geophys. Res. Atmos.*, *122*, 299–317, doi:10.1002/2016JD025527.

Received 16 JUN 2016
Accepted 12 NOV 2016
Accepted article online 16 NOV 2016
Published online 4 JAN 2017

A critical evaluation of modeled solar irradiance over California for hydrologic and land surface modeling

Karl E. Lapo[1], Laura M. Hinkelman[2], Edwin Sumargo[3], Mimi Hughes[4,5], and Jessica D. Lundquist[6]

[1]Atmospheric Sciences Department, University of Washington, Seattle, Washington, USA, [2]Joint Institute for the Study of the Atmosphere and Ocean, University of Washington, Seattle, Washington, USA, [3]Scripps Institution of Oceanography, University of California, San Diego, La Jolla, California, USA, [4]Cooperative Institute for Research in Environmental Sciences, University of Colorado Boulder, Boulder, Colorado, USA, [5]Physical Sciences Division, NOAA Earth System Research Laboratory, Boulder, Colorado, USA, [6]Civil and Environmental Engineering, University of Washington, Seattle, Washington, USA

Abstract Studies of land surface processes in complex terrain often require estimates of meteorological variables, i.e., the incoming solar irradiance (Q_{si}), to force land surface models. However, estimates of Q_{si} are rarely evaluated within mountainous environments. We evaluated four methods of estimating Q_{si}: the CERES Synoptic Radiative Fluxes and Clouds (SYN) product, MTCLIM, a regional reanalysis product derived from a long-term Weather Research and Forecast simulation, and Mountain Microclimate Simulation Model (MTCLIM). These products are evaluated over the Central Valley and Sierra Nevada mountains in California, a region with meteorology strongly impacted by complex topography. We used a spatially dense network of Q_{si} observations ($n = 70$) to characterize the spatial characteristics of Q_{si} uncertainty. Observation sites were grouped into five subregions, and Q_{si} estimates were evaluated against observations in each subregion. Large monthly biases (up to 80 W m^{-2}) outside the observational uncertainty were found for all estimates in all subregions examined, typically reaching a maximum in the spring. We found that MTCLIM and SYN generally perform the best across all subregions. Differences between Q_{si} estimates were largest over the Sierra Nevada, with seasonal differences exceeding 50 W m^{-2}. Disagreements in Q_{si} were especially pronounced when averaging over high-elevation basins, with monthly differences up to 80 W m^{-2}. Biases in estimated Q_{si} predominantly occurred with darker than normal conditions associated with precipitation (a proxy for cloud cover), while the presence of aerosols and water vapor was unable to explain the biases. Users of Q_{si} estimates in regions of complex topography, especially those estimating Q_{si} to force land surface models, need to be aware of this source of uncertainty.

1. Introduction

The incoming solar irradiance (Q_{si}) is the primary energy input for the surface. This energy flux plays a central role in governing the mass and energy cycles at the land surface, for instance providing energy for melting snow [*Cline*, 1997; *Mazurkiewicz et al.*, 2008], potential evapotranspiration [*Gong et al.*, 2006; *Irmak et al.*, 2012; *Cristea et al.*, 2013], and controlling the diurnal cycle of land surface temperature and latent and sensible heat fluxes.

In uncoupled land surface models (LSMs), it is commonly assumed that the uncertainties in land surface model processes are substantially larger than the forcing data errors, often with the meteorological forcing completely neglected as a source of uncertainty [e.g., *Rutter et al.*, 2009]. A number of recent studies have explicitly examined how uncertainty in the Q_{si} data used to force LSMs influences model performance. Uncertainty in Q_{si} has been found to alter parameter selection in a hydrologic model [*Xia et al.*, 2005], cause large differences in simulated high-elevation runoff [*Mizukami et al.*, 2014; *Hinkelman et al.*, 2015], and strongly control the rate of simulated snowmelt [*Lapo et al.*, 2015b]. *Ménard et al.* [2015] concluded that uncertainty in their forcing data, including Q_{si}, was the largest source of uncertainty when considering multiple configurations of the same land model. These studies taken together suggest that uncertainty in Q_{si} estimates can have a substantial impact on land surface modeling.

Uncertainties in forcing data have the potential to create an "insidious data disaster," subtle data errors that inhibit model development and evaluation if they are not accounted for when forcing LSMs [*Lundquist et al.*,

2015]. Therefore, the goals of this study are to characterize the uncertainty in Q_{si} estimates used in studies of land surface processes, provide guidance in the use of these estimates, and to attribute uncertainties in Q_{si} estimates to particular meteorological conditions. In doing so, we also hope to bridge between the communities that develop estimates of Q_{si} and the communities that use these estimates for land surface modeling.

There are numerous methods for estimating irradiances, all of which are used to varying extents within communities that study the land surface. Q_{si} can be estimated by using satellite observations to constrain a radiative transfer model [e.g., *Wielicki et al*., 1998], output from reanalysis [e.g., *Mesinger et al*., 2006], and empirical methods that relate other more commonly observed meteorological variables to Q_{si} [e.g., *Thornton and Running*, 1999]. While the empirical approaches are historically the most common methods in land surface hydrology, Q_{si} estimates from other methods have been used to take advantage of their spatial and temporal continuity [e.g., *Durand et al*., 2008; *Langlois et al*., 2009; *Shi et al*., 2009; *Ménard et al*., 2015] and to capture the patterns of irradiances in sparsely observed regions [e.g., *Simpson et al*., 2004; *Hinkelman et al*., 2015].

However, there is a distinct lack of knowledge about how these estimates perform in mountainous regions. Q_{si} estimates are typically evaluated at a selected number of high-quality sites. This approach is typified by the Radiative Flux Assessment [*Raschke et al*., 2012], in which globally estimated surface irradiances were evaluated at select number of high-quality observation sites. These same sites are repeatedly used in evaluations of estimated irradiances [*Hinkelman et al*., 1999; *Cosgrove et al*., 2003; *Luo*, 2003; *Pinker et al*., 2003; *Schroeder et al*., 2009; *Zhang et al*., 2012; *Bohn et al*., 2013]. creating a disconnect between the location these estimates of Q_{si} are evaluated and the regions in which the estimates are used. In particular, mountainous environments are critical regions in hydrology [*Viviroli et al*., 2007], yet the overwhelming majority of these commonly used evaluation sites are not located in complex terrain. Studies have noted the large uncertainty of Q_{si} within areas of complex terrain [*Hinkelman et al*., 2012; *Raschke et al*., 2012; *Slater et al*., 2013]. However, given the limitations of few observations and the high spatial variability of Q_{si} in regions of complex terrain [*Hakuba et al*., 2013], no conclusion could be drawn on what products perform the best in this environment.

In this study we address the uncertainty and variability of Q_{si} estimates over a study domain with meteorology strongly influenced by topography, the Central Valley and Sierra Nevada Mountains in California. Unique to this study, we employ relatively dense spatial ground observations, enabling us to sample how uncertainty varies spatially (Figure 1). To focus on Q_{si} uncertainty relevant to land surface modeling, we evaluate Q_{si} products that have been or will be used in hydrologic studies in complex terrain: the Mountain Microclimate Simulation Model v4.2 (MTCLIM) [*Thornton and Running*, 1999; *Thornton and Hasenauer*, 2000], the Clouds and the Earth's Radiant Energy System (CERES) synoptic cloud and radiation (SYN) product [*Doelling et al*., 2013; *Rutan et al*., 2015], the North American Land Data Assimilation System (NLDAS) [*Cosgrove et al*., 2003], and a dynamically downscaled data set generated using the Weather Research and Forecast (WRF) model with the North American Regional Reanalysis (NARR) [*Mesinger et al*., 2006] as lateral boundary conditions, similar to that documented in *Hughes et al*. [2012]. We target mean differences in Q_{si}, which have been found to have much larger impact on snow models than random errors [*Lapo et al*., 2015b; *Raleigh et al*., 2015]. Finally, we attribute uncertainty in Q_{si} to specific meteorological conditions.

In section 2 we describe the study domain and its typical meteorological patterns (section 2.1), our approach of using a spatially dense network of lower quality observations (section 2.2), the ground observations (section 2.3), the regional classification of the ground observations (section 2.4), and the methods for estimating Q_{si} evaluated in the study (section 2.5). In section 3 we present results on how estimates of Q_{si} evaluate against ground observations (section 3.1). These results are discussed in section 4, specifically addressing patterns of uncertainty in Q_{si} (section 4.1), attributing errors in Q_{si} to particular meteorological conditions (section 4.2), and providing guidance on selecting estimates of Q_{si} (section 4.3).

2. Data and Methods

2.1. Study Domain

Areas of complex topography are characterized by unique meteorological conditions that influence Q_{si}: reoccurring cloud patterns such as afternoon thunderstorms [*Olyphant*, 1984] and mountain wave clouds [*Grubišić and Billings*, 2008], topographically driven gradients in water vapor [*Feld et al*., 2013], stable inversions causing persistent fog [*Underwood et al*., 2004; *Lundquist and Cayan*, 2007; *Baldocchi and Waller*,

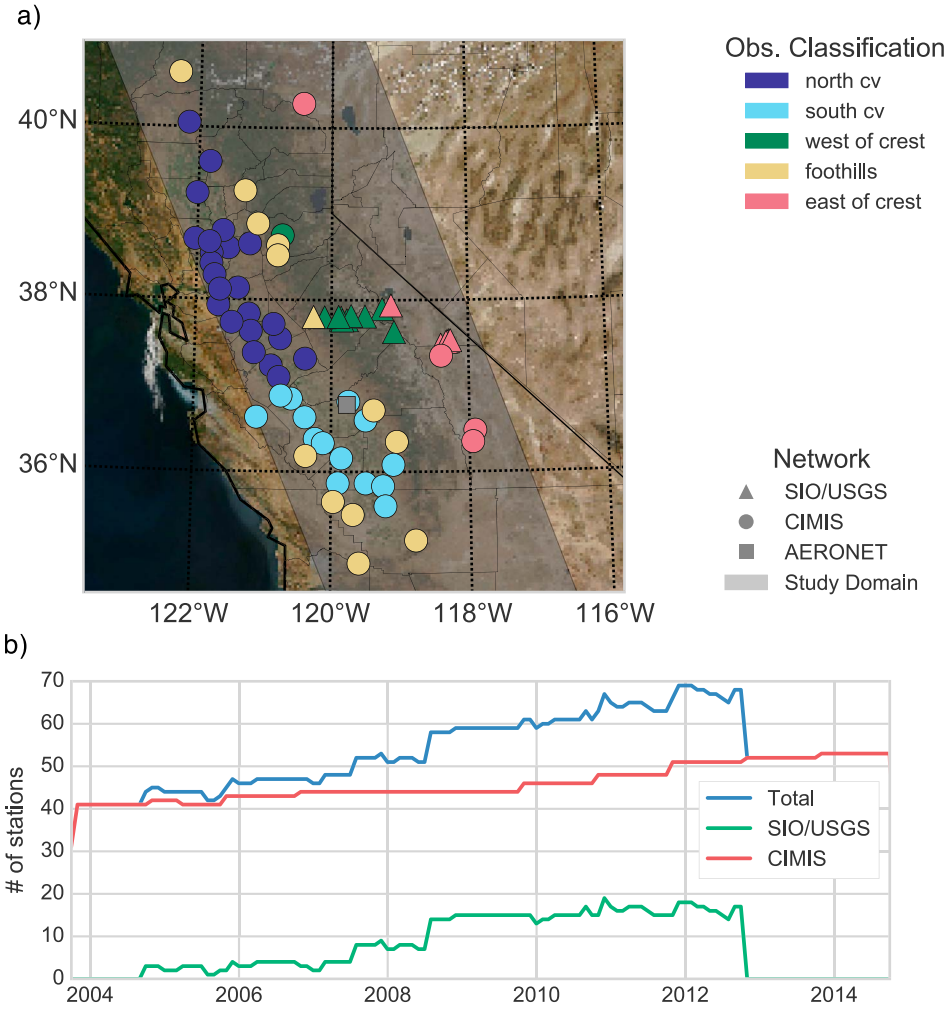

Figure 1. (a) The California study domain with observations grouped by region classification and network (see text). (b) The number of ground observations available during each month after quality control screening.

2014] and trapping aerosols [*De Young et al.*, 2004; *McMeeking et al.*, 2006], and reduced optical depths from water vapor, aerosols, and air mass due to higher elevations [*Marty et al.*, 2002; *Yang et al.*, 2010].

The typical meteorological conditions of the study domain and how they are expressed by surface measurements of Q_{si} are demonstrated with Moderate Resolution Imaging Spectroradiometer (MODIS) mosaic images (worldview.earthdata.nasa.gov) overlaid with the observed daily irradiances (section 2.3, Figure 2). Clear-sky conditions are commonly found over the California study domain. Even during clear-sky conditions, substantial spatial variability in the observed irradiance exists due to the influence of water vapor and aerosols (Figure 2a), highlighting the large variability between neighboring stations that can occur even in the absence of clouds. This spatial variability between closely located stations, even under clear-sky conditions, has been noted in the past [*Wang et al.*, 2012]. The Central Valley is well known for its radiation fog, or tule fog, that occurs during the winter [*Baldocchi and Waller*, 2014]. The air near the surface cools at night, forming fog that can reach up to 300 m in height but still remains confined to the Central Valley [*Underwood et al.*, 2004]. An example of tule fog is shown in Figure 2b, with a sharp gradient between low-elevation valley stations within the fog and those outside it, leading to a difference of an order in magnitude in observed Q_{si} values. Similar to tule fog, aerosols can become trapped in the Central Valley [*Ying and Kleeman*, 2009]. While there are higher aerosol concentrations during the winter [*Zhang and Anastasio*, 2001], the summer sees the largest aerosol optical depths due to the influence of wildfires [*Lewis et al.*, 2010]. In Figure 2c, smoke, likely from wildfires, accumulated in the southern Central Valley and is visible as a haze in the MODIS mosaic. There is no clear signal of the aerosol asymmetry between the north and south of the valley in the mean Q_{si}

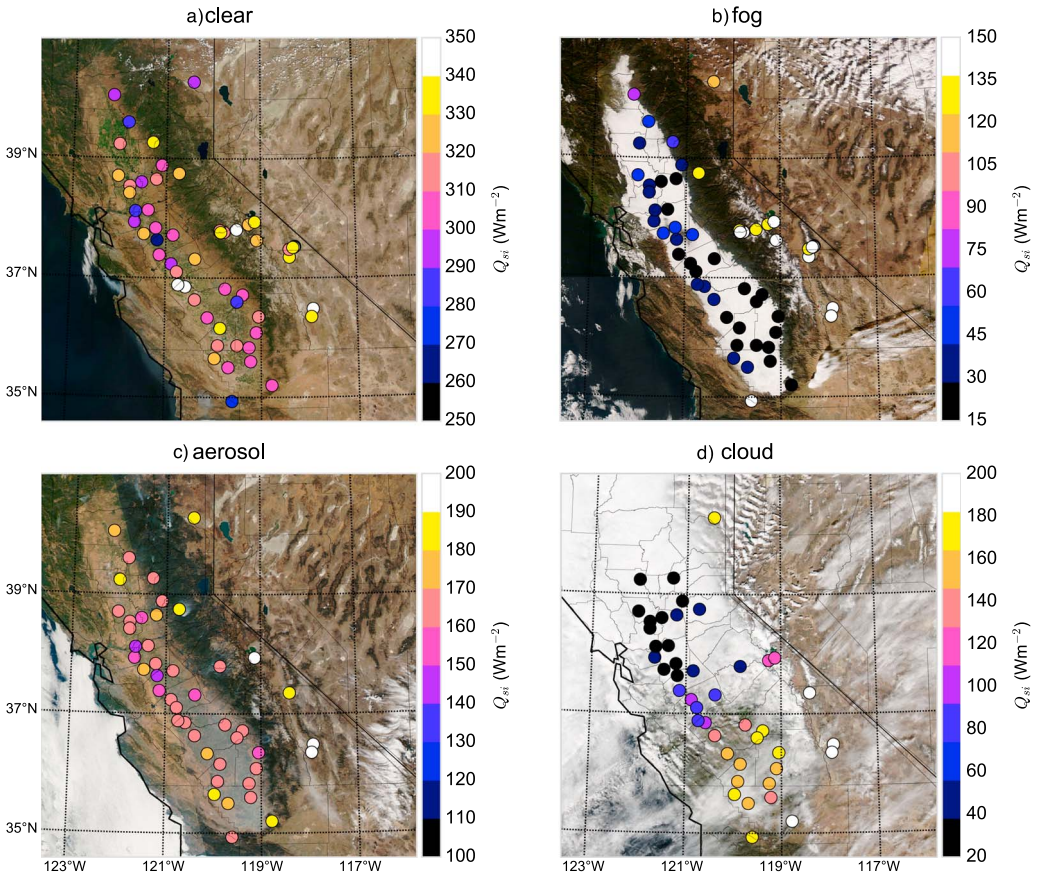

Figure 2. Example of common meteorological features as observed by mosaic images of MODIS corrected surface reflectances with daily mean observations of Q_{si} for (a) clear conditions (15 August 2009), (b) radiation fog within the valley (3 December 2008), (c) a day with high aerosol concentrations (23 October 2005), and (d) a day during a large, synoptically driven precipitation event over California (6 March 2006).

observations, but a clear difference between the valley sites and the mountain sites is evident. Finally, California's precipitation is strongly seasonal, with the majority occurring in the winter [*Finkelstein and Truppi*, 1991] during atmospheric river events [*Dettinger et al.*, 2011; *Rutz et al.*, 2014]. These synoptically driven events lead to widespread stratocumulus cloud cover across the study domain. In contrast, clear days (Figure 2a) dominate the summer and shoulder seasons. Spatial gradients in this cloud cover can lead to an order of magnitude difference in the daily Q_{si} observed by the surface stations, as demonstrated in Figure 2d. The sharp gradient in cloud cover in Figure 2d (cloudy in the west, clear in the east) along the crest of the Sierra Nevada is a commonly observed feature.

2.2. Using a Dense Network of Lower Quality Observations

In order to understand how Q_{si} varies over the complex topography of the study domain, we require a relatively dense spatial distribution of surface observations. Prior evaluations mainly used isolated observation sites, such that no conclusions could be drawn regarding the spatial patterns [e.g., *Slater et al.*, 2013; *Hinkelman et al.*, 2015]. Typically, it is assumed that neighboring stations experience different meteorological conditions at shorter (e.g., daily) time scales but similar conditions when considering longer time scales (e.g., monthly or annual) [*Wang et al.*, 2012]. However, this assumption is less straightforward in mountainous environments, for instance due to orographically driven cloud patterns. Spatial variability in Q_{si} has been found to be much higher in regions of complex terrain [*Hakuba et al.*, 2013], with other studies noting large differences in Q_{si} between closely located low- and high-elevation sites, notably due to differences in cloud amount [*Iziomon et al.*, 2001; *Marty et al.*, 2002], as shown in Figure 2d.

Estimating spatial patterns of Q_{si} requires a departure from the typical approach of using high-quality but isolated stations. Instead, we must rely on "second tier" observations. The large majority of shortwave

observations in mountainous environments are unable to meet World Meteorological Organization (WMO) guidelines for moderate quality [*World Meteorological Organization*, 2008] (for an exhaustive list of networks that observe Q_{si} across the continental U.S., see *Slater* [2015]), namely failing to meet the requirements for daily inspections and appropriate instrumentation. These stations have substantially larger uncertainty associated with their Q_{si} observations, especially in mountains as conditions typical of these environments, such as extensive shading by topography and vegetation, snow obscuring pyranometer domes, tilting, limited access for maintenance, and thermal offsets, create observational uncertainties not frequently encountered in other climates.

We have developed methods for quality controlling observations from sites that do not meet WMO guidelines, described in the supporting information. Specifically, we identify and remove periods of shading caused by both vegetation and topography, periods with snow obscuring pyranometer domes [*Lapo et al*., 2015a], and thermal leaking [*Philipona*, 2002], in addition to screening for nonphysical observations [*Long and Shi*, 2008]. These quality control methods require specific observations to function: hourly observations of Q_{si}, air temperature, wind speed, and precipitation. These methods are unable to identify sensor drift, necessitating the use of observations that receive regular maintenance. To compensate, we take advantage of the expected similarity between observations that experience similar meteorology to remove observations that do not match nearby stations in the long-term mean. These quality control methods allow the diagnoses of particular observational errors in order to make use of these otherwise underutilized data. All code for running these quality control methods is freely available (github.com/Mountain-Hydrology-Research-Group/moq).

Other studies that have examined Q_{si} spatial variability over large regions have also needed to use lower quality observations. Using these lower quality observations requires extensive quality control [*Tang et al*., 2010; *Slater*, 2015]. The approach taken by Tang et al. and Slater to address the additional uncertainty from these "second tier" observations was to screen observed Q_{si} values using modeled clear-sky values. As a result, both studies strongly rely on the accuracy of their modeled clear-sky Q_{si}. Slater scales observations within some tolerance of the modeled clear-sky values to match the modeled values. This approach, while accounting for calibration differences between sites, limits the analysis to only periods that are relatively clear. Similarly, Tang et al. note that their method likely is not applicable to regions of high pollution or dense cloud cover. Additionally, Tang et al. use their modeled values to fill gaps within their data. These approaches may lead to some circularity in the evaluation of Q_{si} estimates: observations are screened to match modeled values, which are then used to evaluate modeled irradiances. There are clear difficulties associated with using lower quality observations, but in many areas these observations are all that are available. Future research would strongly benefit from an explicit examination of how different quality control methods perform relative to trusted observations.

2.3. Ground Observations

Surface observations come from two networks: the California Irrigation Management Information System (CIMIS), operated by the California Department of Water Resources, and the Scripps Institution of Oceanography (SIO) hydroclimate network, jointly operated by SIO and the United States Geological Survey (Figure 1). These stations are roughly split between the Central Valley and Sierra Nevada, respectively. The stations are grouped according to the meteorology of each region (section 2.4).

2.3.1. CIMIS

The CIMIS network is designed to estimate the evaporative demands for irrigators. The CIMIS observations were obtained through the University of California Integrated Pest Management (IPM) weather station network (ipm.ucdavis.edu). The data include extensive metadata, including site environment, maintenance, and filling methodology of missing data. Questionable and missing data are filled from a neighboring station that is judged to have similar meteorological conditions, providing a temporally complete daily time series for each station.

The 54 CIMIS stations used in this study are located mostly within the Central Valley, with some in the foothills of the Sierra Nevada (Figure 1a) with most of the observations available prior to the start date of the study period (Figure 1b). Q_{si} observations are made with LI-COR® LI200X pyranometers. Silicon sensors, such as these, are known for their lower accuracy compared to thermopile instruments, especially due to nonlinear spectral response [*Sengupta et al*., 2012; *Vignola et al*., 2014]. Further complicating instrument uncertainty,

corrections developed at low elevations are not applicable to high elevations [*Sengupta et al.*, 2012]. Precipitation is also observed at the CIMIS stations.

2.3.2. Scripps

The SIO hydroclimate network was designed to fill the gaps between the California Department of Water Resources stations along an east-west transection of the Central Sierra Nevada. The observations are arranged to investigate the elevational gradients of Q_{si} and other meteorological measures across the transect. Locations were chosen such that topographic- and tree-shading effects are minimized, but not entirely removed (supporting information). The other measures available from the network include air temperature and pressure, relative humidity, wind speed, and precipitation. The observations were provided by the SIO Hydroclimate Group.

The Q_{si} observations are made with LI-COR® LI-200SA pyranometers. The pyranometers are factory calibrated and replaced approximately every 2 years. The installation started in 2004 with only three stations, and more stations were gradually added to the network in the following years (Figure 1b). The observations are mostly available post-2008. Of the 18 SIO stations used in this study, 10 stations are located along the Tioga Road (a part of California State Route 120) in Yosemite National Park. Other stations are installed in the White Mountain (seven stations) and Devil's Postpile National Monument (one station) areas. Unlike CIMIS, the SIO data sets were provided as raw data, which means no quality control had been performed. Thus, quality control procedures were applied to address the issues of missing data and snow- and topographic/tree-shading-related errors. These quality control techniques allow us to place a greater confidence in the mountain observations.

2.3.3. Aerosol Robotic Network

Potential sources of uncertainty in Q_{si} estimates include aerosols and water vapor. To test how those quantities influence estimated Q_{si}, we use observations from the Aerosol Robotic Network (AERONET, aeronet.gsfc.nasa.gov) [*Holben et al.*, 1998] Fresno station (36.78°N, 119.77°W, 0 m, Figure 1a). Total aerosol optical depth and precipitable water vapor are derived from the cloud-screened level 2.0 Sun photometer data.

2.4. Observation Subregions

Based on the meteorological features of this study domain we classify observation sites into geographic regions. This grouping of stations enables comparisons both between stations where we expect similarities in observed Q_{si} values for quality control purposes (supporting information) and region-specific comparisons between estimated and observed Q_{si}. Observation sites are classified into five groups (Figure 1a): (1) South Central Valley (SCV): Central Valley stations (elevation $<$ 100 m) south of 37 N; (2) North Central Valley (NCV): Central Valley stations (elevation $<$ 100 m) north of 37 N; (3) Foothills (FHLLS): stations outside the influence of the Central Valley yet still in the foothills elevations of the Sierra Nevada (100 m $<$ elevation $<$ 800 m); (4) East of Crest (EC): mountain stations (elevation $>$ 800 m) east of the crest of the Sierra Nevada; and (5) West of Crest (WC): mountain stations (elevation $>$ 800 m) west of the crest of the Sierra Nevada.

We assign uncertainty to the ground observations based on how the Q_{si} observations spread within each group. The monthly standard deviation of Q_{si} among stations within a group is composited by month, yielding a time varying uncertainty for each region (grey region in Figure 3). Biases at the monthly scale between the observations and products below these uncertainty thresholds are considered insignificant, as the observations themselves spread by a larger amount.

2.5. Estimated Irradiances

Estimated irradiances are matched to surface observations by extracting the grid cell containing the surface station for each product. Products are compared to observations within a region, thereby explicitly focusing on the mean irradiance within a region, rather than an individual station. A regional analysis with multiple stations limits issues of spatial representativeness that have been found in regions of complex terrain [*Hakuba et al.*, 2013]. As such, we do not expect that the representativeness of the different spatial scales of the estimated irradiances is an issue in this analysis.

2.5.1. CERES SYN

CERES SYN is a global 1° gridded surface irradiance product with a temporal resolution of 3 h that includes both upwelling and downwelling irradiances [*Rutan et al.*, 2015]. The SYN surface radiative fluxes are

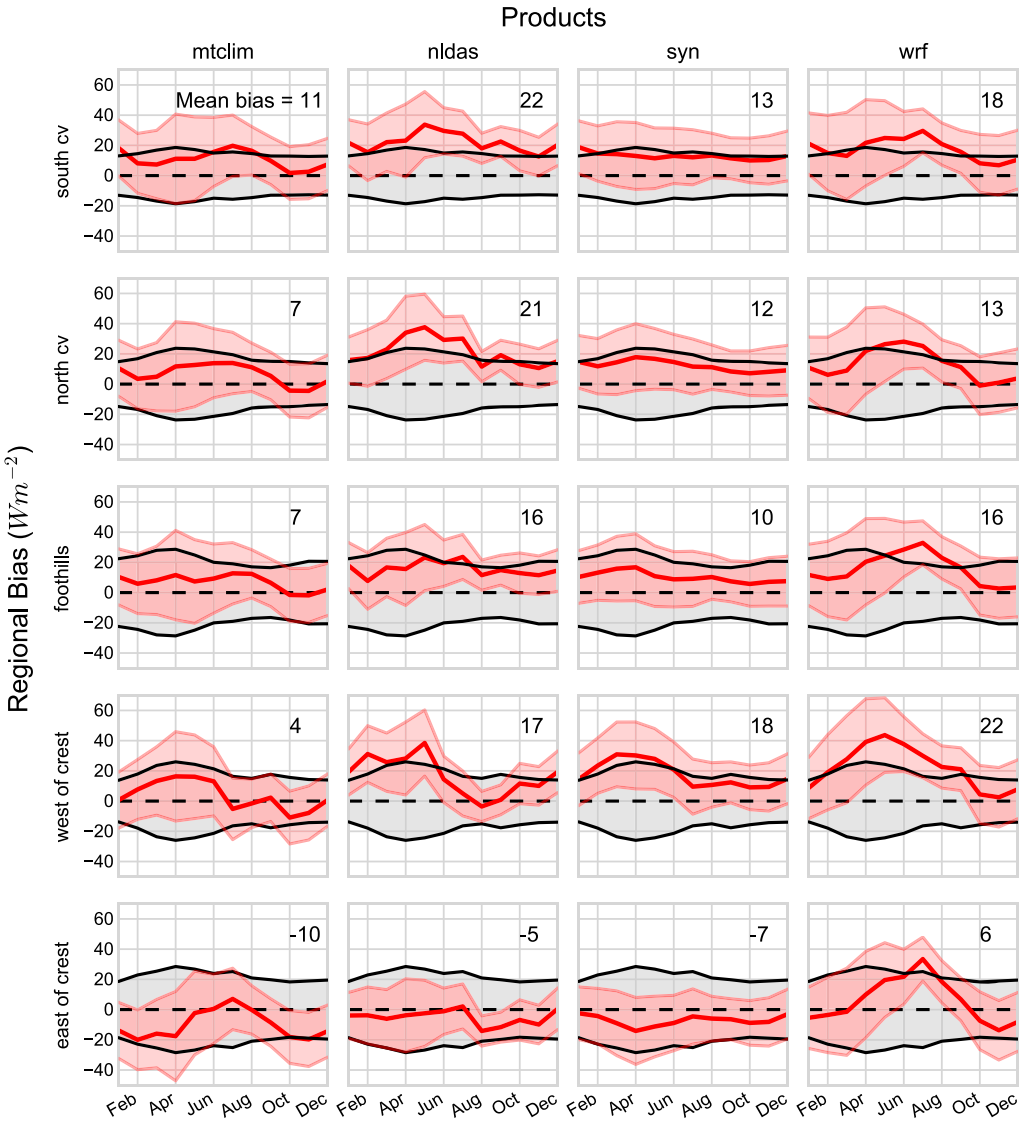

Figure 3. Composited monthly biases in Q_{si} for all products (columns) and regions (rows, Figure 1). The thick red line is the mean bias for each month, and the red region is the mean standard deviation of the product for that month and region. The grey region is the estimated observational uncertainty, based on the composited monthly standard deviation of observations within each group. The number in the upper right hand corner of each subplot is the mean bias over the entire study period.

computed by applying a two-stream radiative transfer model [*Fu and Liou*, 1993; *Kato et al*., 2005] to a description of the atmospheric column that is based primarily on satellite observations. Cloud properties are provided by MODIS 4 times a day. Between MODIS overpass times, cloud properties are derived from 3-hourly geostationary satellite measurements that have been carefully calibrated to match the MODIS measurements [*Doelling et al*., 2013]. Thus, the output fluxes reflect both the daily solar cycle and its modification by changing cloud conditions. We use the recommended "untuned" values from SYN [*Rutan et al*., 2015]. SYN was also recently evaluated in mountainous environments using observations that had been quality controlled using the techniques described in this paper [*Hinkelman et al*., 2015]. We use SYN data for the period July 2002 to May 2014.

2.5.2. NLDAS

The North American Land Data Assimilation (NLDAS) project provides data sets to support land surface modeling studies, with the specific goal of improving simulations of soil moisture. NLDAS Q_{si} is available 1979-present at 1/8° and hourly resolution [*Cosgrove et al*., 2003]. Q_{si} values are found by downscaling output from

the North American Regional Reanalysis (NARR) 32 km spatial grid and 3 h times step to the NLDAS resolution. The downscaled NLDAS Q_{si} fields are bias corrected based on the ratio of monthly irradiances from a GOES satellite-derived and NARR Q_{si} [*Cosgrove et al*., 2003]. The downscaled values are technically instantaneous, and not hourly averages, although it is unclear how much this distinction impacts the values obtained from NLDAS. NLDAS is a common source of data for snow hydrology studies, especially reconstructions of the snow water equivalent (SWE) [*Durand et al*., 2008]. We use NLDAS data from the period January 2004 to December 2010.

2.5.3. Regional WRF Simulations

The regional WRF simulations were generated using WRF version 3.6.0 [*Skamarock et al*., 2008] to dynamically downscale NARR, with a methodology very similar to that used in *Hughes et al*. [2012]. The WRF downscaling had two nested domains, with an outer 18 km grid extending across the northeastern Pacific and much of the U.S. intermountain west, and a 6 km domain that covers all of California (similar to Figure 1 in *Hughes et al*. [2012]). Both domains had 82 vertical levels, with ~50–75 m resolution within the lowest 2 km of atmosphere, with model top at 100 hPa. Both domains use Morrison double-moment microphysics [*Morrison et al*., 2009], Dudhia shortwave radiation [*Dudhia*, 1989] and Rapid Radiative Transfer Model (RRTM) longwave radiation [*Mlawer et al*., 1997] called every 6 min, Kain-Fritsch convective parameterization [*Kain*, 2004], Yonsei University planetary boundary layer scheme [*Hong et al*., 2006], and Noah land surface model [*Tewari et al*., 2004]. Tmodel was initialized 3 h prior to 0 UTC on the 1st, 6th, 11th, 16th, 21st, and 26th of each month, with the first 3 h discarded as spin-up, and run through 0Z of the next time period (i.e., run for 5 days, 3 h, except at the end of each month, which differs based on month length). We use WRF Q_{si} for the period January 2004 to December 2014.

2.5.4. MTCLIM

We use MTCLIM as implemented in the Variable Infiltration Capacity (VIC) Macroscale Hydrologic Model v4.2b [*Liang et al*., 1994]. MTCLIM relates the diurnal temperature range, relative humidity, and precipitation to Q_{si} through the Thornton-Running empirical method [*Thornton and Running*, 1999; *Thornton and Hasenauer*, 2000]. Gridded meteorological data for running MTCLIM over the study area were obtained from the *Livneh et al*. [2014] data set. Historically, empirical algorithms, such as MTCLIM, are the most commonly used methods to force LSMs.

There are considerable differences between versions 4.2 and 4.3 of MTCLIM. VIC implements version 4.3 of MTCLIM. However, the version 4.3 features, namely the bias correction to Q_{si} in the presence of snow and iterative solutions to humidity, are turned off by default. Effectively, turning these features off means that MTCLIM within VIC is version 4.2 (T. Bohn, personal communication, 2016). Given the confusion regarding which version of the algorithm is available and the difference in performance between the two versions, we caution future users of MTCLIM. *Bohn et al*. [2013] evaluated MTCLIM against selected high-quality observations and found that version 4.2 performed well for noncoastal sites, a result supported by *Slater* [2016]. In our study we use MTCLIM to refer to MTLCIM v4.2 forced by the Livneh data. MTLCIM is available at 1/16° spatial resolution for the period January 2000 to December 2011.

3. Results

3.1. Evaluation

The composited monthly mean Q_{si} from the products is compared to the observations for each study subregion (Figure 3). Products yield a positive bias for most groups and seasons. Generally, MTCLIM and SYN both yield group biases less than the estimated observational uncertainty, while NLDAS and WRF more frequently have larger, positive biases outside the range of estimated observational uncertainty.

All products display some seasonality in their biases; typically the largest biases occur in the spring or late summer (Figure 3). WRF and NLDAS generate the most prominent seasonal cycle in bias, with the months with the largest mean bias exceeding the estimated observational uncertainty. The seasonality does not always hold, for instance all products have a magnitude of bias that is roughly equal for all seasons during 2004 (Figure 4). However, this lack of seasonality in the Q_{si} bias means a seasonal cycle in the bias of transmissivity, and vice versa.

When considering the mountain groups, MTCLIM produces the smallest biases (Figure 3). The other three products all yield positively biased Q_{si} outside the estimated observational uncertainty for the WC group, with mean biases reaching 40 W m^{-2}. There is a striking difference between the biases for the EC and WC stations

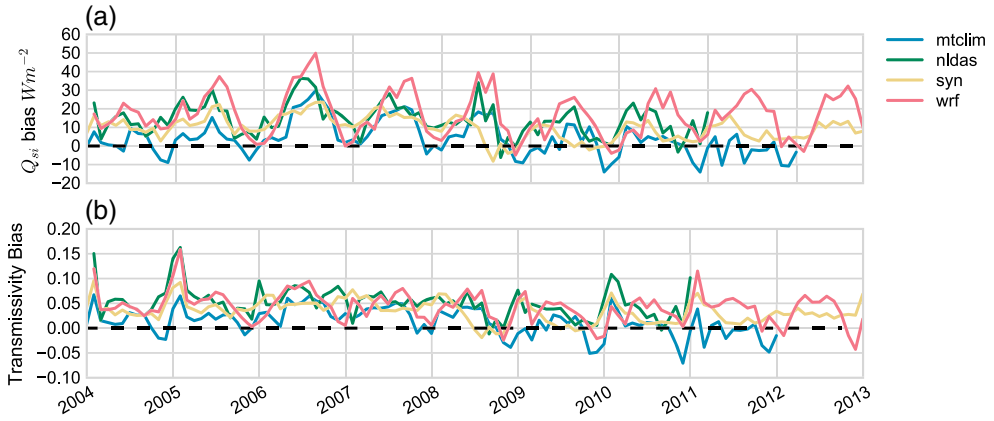

Figure 4. The mean bias in (a) Q_{si} and (b) transmissivity for each product over the entire study area.

(Figure 3). The products evaluate to a positive bias for WC, with smaller, and even negative biases at EC stations. WRF produces the strongest seasonality in bias, spanning the range of estimated observational uncertainty for the EC group and exceeding the estimated observational uncertainty in the WC group.

Certain periods appear more difficult to accurately simulate. Most prominently, there are large biases during the early spring to summer in 2006–2008 (Figure 4). The spring of 2006 is especially noteworthy as this period sees the largest biases during the study period and will be explored in detail in section 3.2. Others have noted 2006 and 2007 as being years with many atmospheric river events [*Guan et al.*, 2010], potentially suggesting that those events may drive the uncertainty.

3.2. Spatial Patterns

The spatial patterns of biases are examined for the entire domain, using the mean irradiances during May 2006 (Figure 5). We examine this period in detail since the spring of 2006 contains some of the largest biases in this study (Figure 4). Ground observations show low irradiances in the Central Valley and up the western flank of the Sierra Nevada. A gradient in observed Q_{si} is evident between observations at sites on opposite sides of the Sierra Nevada crest, coinciding with a clear difference in biases between EC and WC stations. All products demonstrate high monthly biases (exceeding 50 W m^{-2}) at the majority SCV and some NCV stations where low Q_{si} values are observed. In contrast, Q_{si} estimates from each product have smaller positive, or even negative, biases for the EC and the NCV stations that observe larger Q_{si} values.

Figure 5 highlights that the large biases during 2006 (Figure 4) are not the result of individual stations but a region wide result. For example, the low Q_{si} values observed by WC stations are not limited to a single station but are prevalent across the entire group. This result is consistent across all months of the spring and summer in 2006 (results not shown). Substantial differences between products are apparent even without the comparison to the surface observations, especially over the western flank of the Sierra Nevada. However, the differences in spatial pattern over the Sierra Nevada occur where we lack surface observations; errors in Q_{si} cannot be fully assessed at higher elevations.

3.3. Q_{si} Uncertainty at High Elevations

To understand the differences in how each product represents Q_{si} over the entire study domain, especially high elevations, we examine the mean difference between each product and MTCLIM. To facilitate this comparison, all products are interpolated to WRF's spatial resolution (6 km, the finest spatial resolution among the four products) using a nearest neighbor approach. For each grid cell, the difference between each product and MTCLIM (product-MTCLIM) is found and seasonally composited (Figure 6). We chose to compare against MTCLIM since it best matches observations in all groups (Figure 3). Differences between each product and MTCLIM are the smallest in winter and fall and largest in the spring and summer. The seasonal cycle in differences may be expected due to the overall lower Q_{si} in the fall and winter and higher Q_{si} in the spring and summer. LSMs are sensitive to the absolute, rather than relative, bias motivating our focus on mean differences between products [*Lapo et al.*, 2015b; *Raleigh et al.*, 2015].

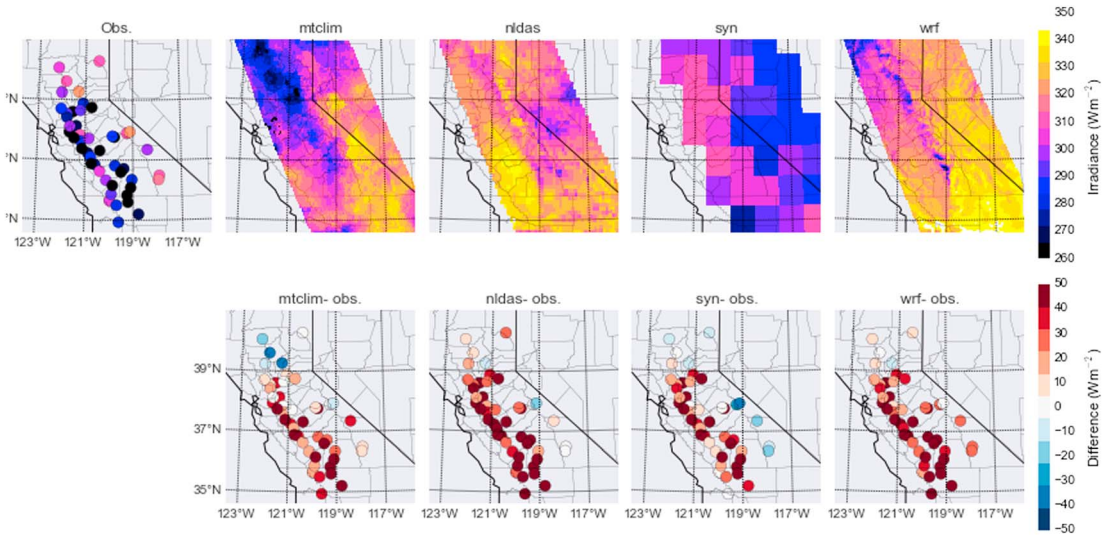

Figure 5. (top row) Maps of monthly mean irradiance for observations and all radiation products over the entire study domain during May 2006. (bottom row) The bias (estimate-observation) between each radiation product and ground observations is also shown.

The domain-wide differences from MTCLIM appear to be closely associated with topography, with many topographic features, such as the Sierra Nevada, visible in the difference maps (Figure 6). Differences are the largest over the western Sierra Nevada for all products. SYN most closely agrees with MTCLIM, albeit the effect of the large spatial resolution of SYN is evident. NLDAS and WRF strongly disagree with MTCLIM over the western flank of the Sierra Nevada, with disagreement exceeding 50 W m^{-2} in WRF. These maps of differences between each product and MTCLIM highlight that uncertainty in Q_{si} is largest at high elevations to the west of the crest of the Sierra Nevada during the spring.

To further demonstrate the difference in Q_{si} at high elevation between products, we repeat this exercise by analyzing the mean Q_{si} from each product over three example basins (Figure 7). The American basin was selected since it was the focus of intensive hydrologic studies [*Ralph et al.*, 2013], while the Kern and Tuolumne are being studied through the Airborne Snow Observatory [*Painter et al.*, 2015]. Each basin's mean Q_{si} is found by selecting the grid points within each basin's boundary. To facilitate comparison, we present differences from MTCLIM in monthly composited Q_{si} (Figure 7).

The products yield large differences in mean Q_{si} for all basins, disagreeing by as much as 60 W m^{-2} for the American, 80 W m^{-2} for the San Joaquin, 50 W m^{-2} for the Kern, and 70 W m^{-2} for the Tuolumne basin, with the largest disagreements in basin Q_{si} occurring in the early spring to summer. The mean difference in Q_{si} over each basin is typically less than these values, with the mean difference for the entire period between MTCLIM and NLDAS ranging between 7 and 22 W m^{-2}, SYN ranging between −1 and 19 W m^{-2}, and WRF ranging between 20 and 27 W m^{-2} for the three basins. These differences are substantial considering the large area and time being averaged over.

3.4. What Factors Contribute to the Largest Biases?

In order to understand what conditions lead to the largest disagreement, we scale all observations using the top of atmosphere irradiance (equation (1)).

$$T = Q_{si}/S_{\mathrm{TOA}} \tag{1}$$

The transmissivity, T, gives the fraction of the solar irradiance at the top of the atmosphere (S_{TOA}) that is received at the surface (Q_{si}). Transmissivity is not a perfect scaling, as it does not take into account changes in the air mass optical depth at larger solar zenith angles, but it does facilitate comparison across different times of year by reducing the influence of the annual cycle (Figure 4). A reference T for each day of the year is found by compositing T by month and then interpolating the monthly values to a daily scale, facilitating a clean composite of transmissivity for each day of year. The daily transmissivity anomaly (ΔT) at each station is found by subtracting the group reference value from each measured value. ΔT is classified into three groups:

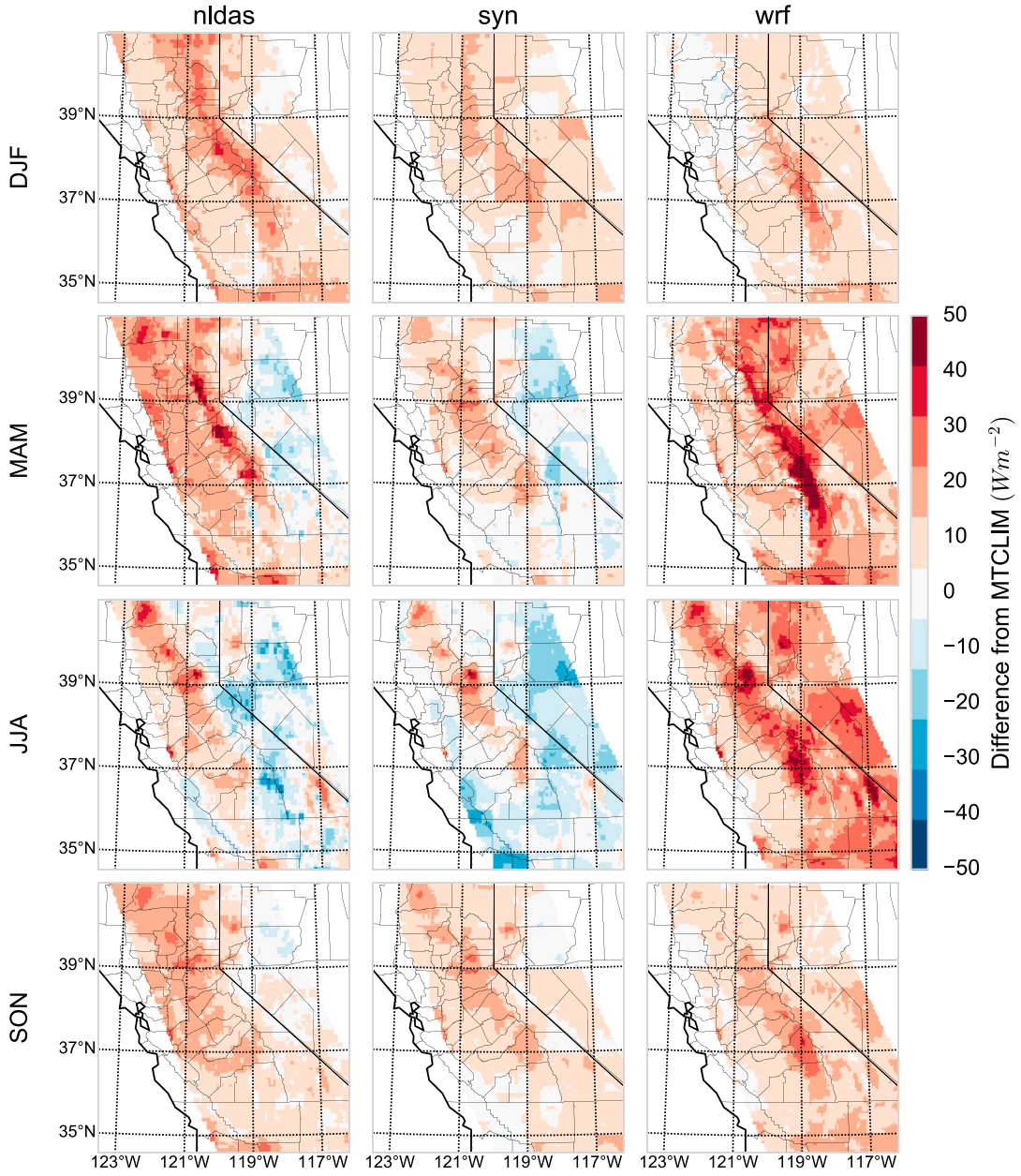

Figure 6. Seasonal composites (winter: December, January, February; spring: March, April, May; summer: June, July, August; fall: September, October, November) of the mean difference over the entire study period between each product and MTCLIM. All products have been regridded using a nearest neighbor approach to a common grid of 6 km, matching the resolution of WRF, which has the finest spatial resolution.

darker than normal conditions ($\Delta T < -0.1$), normal conditions ($-0.1 < \Delta T < 0.1$), and brighter than normal conditions ($\Delta T > 0.1$).

Using the ΔT categories, daily Q_{si} biases are categorized for each observation group (Figure 8). The mean bias during normal conditions is near zero for all products and groups. Similar results are found during brighter than normal conditions ($\Delta T > 0.1$). In contrast, large biases occur during darker than normal conditions, with a mean daily bias close to 50 W m^{-2} for all products except MTCLIM and all groups except the EC group. Darker than normal conditions are associated with the largest biases. This leads to question of which meteorological conditions in Figure 2 cause the largest biases during these darker than average conditions. We test whether the presence of water vapor, aerosols, or clouds is associated with the large biases seen during anomalously dark conditions.

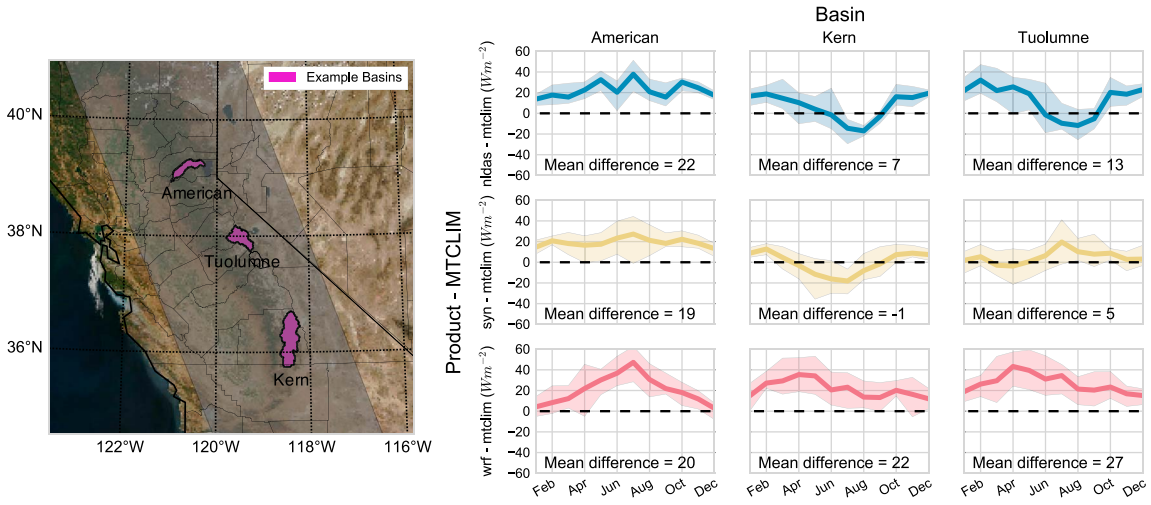

Figure 7. Composited monthly differences in Q_{si} (right) between each radiation product and MTCLIM for grid points within the (left) example basins depicted. The dark line is the mean monthly value, and the shaded region shows all values for the study period.

Aerosol optical depth (AOD) and precipitable water vapor (PWV) are observed at the Fresno AERONET station (Figure 1a). This station falls within the SCV group, so only SCV stations are used for this analysis. Additionally, these observations are only made during days with clear skies. We select for days with a large aerosol or water vapor influences using the criterion of values greater than the median of the AERONET observations. We use the occurrence of precipitation as a proxy for cloudy conditions, since precipitation provides a definitive indicator of cloud presence and cloudy days largely coincide with precipitation in this study domain. Similar to the aerosol and water vapor screening, daily biases and transmissivity anomalies are categorized according to whether any station in each group received precipitation.

Density plots of the daily SCV group bias and transmissivity anomaly are shown in Figure 9. The relationship between negative transmissivity anomalies and positive biases is apparent in the density plot of all

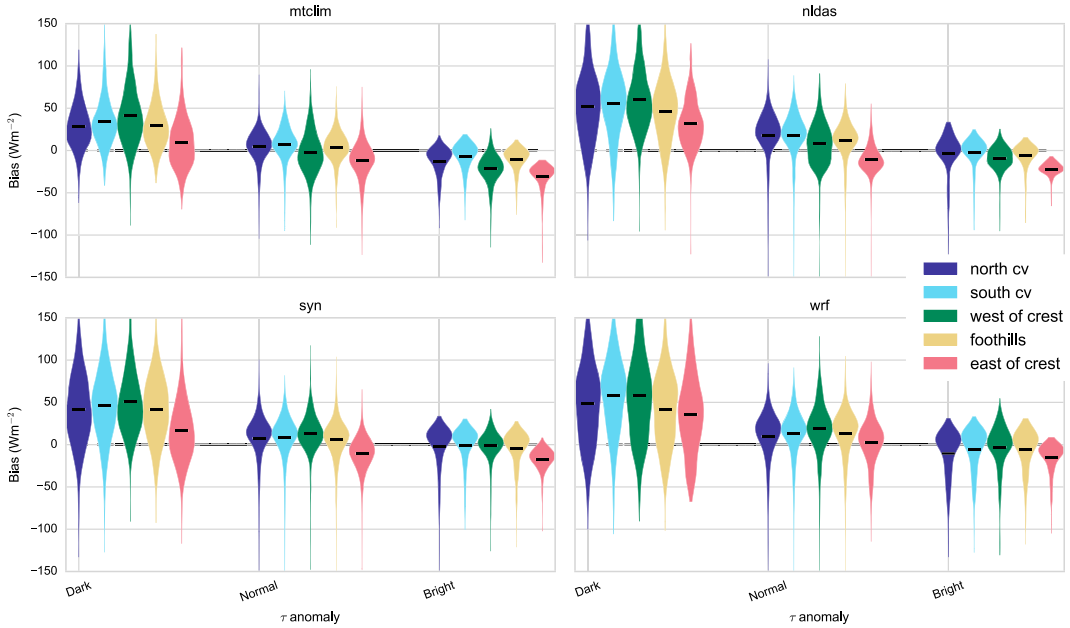

Figure 8. Violin plots of the distribution of daily biases in Q_{si}, binning the data according to the daily transmissivity anomaly into clear (transmissivity anomaly > 0.1), normal (transmissivity anomaly between -0.1 and 0.1), and dark (transmissivity anomaly less than -0.1) bins for each ground observation group (colors) and radiation product (subaxes). The violin plots show the relative distribution of biases through the width of the plot, with the mean bias indicated by the thick black bar.

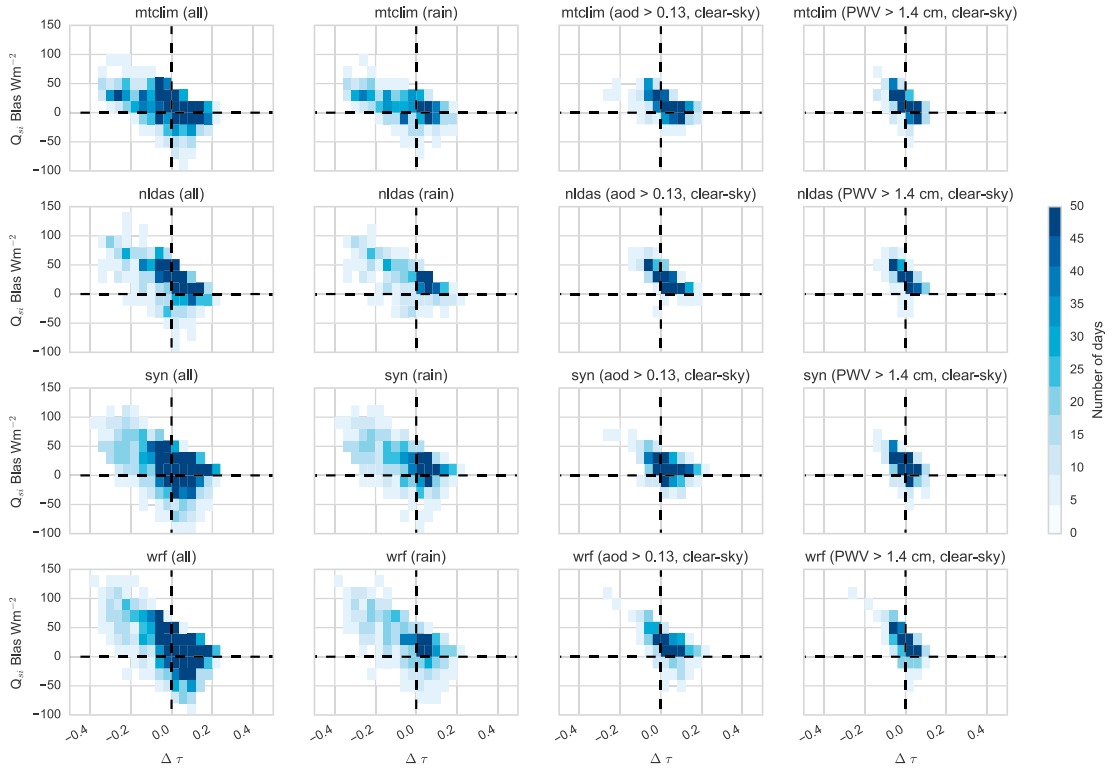

Figure 9. Density plots of daily bias (product-observation) and the anomaly in daily transmissivity for the southern central valley group. Each column shows the transmissivity anomaly and bias for various conditions: all observations, days with rain, days with substantial aerosol (aerosol optical depth > 0.13) and clear skies, and days with substantial water vapor (precipitable water vapor > 1.4 cm) and clear skies. Aerosol optical depth (AOD) and precipitable water vapor (PWV) are both observed by the Fresno AERONET station during clear-sky conditions only.

observations. Days with a negative transmissivity anomaly almost exclusively have a positive bias, whereas days with small or positive transmissivity anomalies have both negative and positive Q_{si} biases.

The presence of large PWV does not correspond to negative transmissivity anomalies, as large PWV occurs almost exclusively on days with $\Delta T > -0.1$. Days with large AOD and clear skies do have a relationship between ΔT and bias. However, days with large AOD mostly coincide with positive transmissivity anomalies, suggesting that aerosols are largely not responsible for the negative transmissivity anomalies and positive biases seen in Figure 8. Days with precipitation are more strongly associated with negative transmissivity anomalies and large, positive biases for all products. The relationship between precipitation and positive biases is consistent across all observational groups (not shown).

4. Discussion

We laid out three primary goals for this study: (1) to describe the uncertainty of Q_{si} estimates in settings where they might be used in studies of land surface processes in complex terrain, (2) to attribute errors to particular meteorology, and (3) to provide guidance in the use of Q_{si} estimates.

4.1. Q_{si} Uncertainty

We interpret both biases outside the observational uncertainty and disagreements between products as indicative of uncertainty in Q_{si}. Spread among the different estimates of Q_{si} indicates uncertainty in the estimated value, since the different values of Q_{si} from each product cannot each be correct.

Uncertainty in Q_{si} is not constant through time. Certain periods, such as spring of 2006, yield high biases for all estimates, with NLDAS and WRF reaching biases of ~60 W m^{-2} across large portions of the study domain (Figure 5). Further, uncertainty in estimated Q_{si} appears to be largest in the spring and summer, which likely has substantial implications for hydrologic modeling due to the sensitivity of evapotranspiration and snow

melt to Q_{si} during this time of year. Uncertainty in the spring and summer is further found in the disagreement between products (Figures 6 and 7). Finally, all products evaluate to large biases (approximately 50 W m^{-2} in magnitude) during darker than normal periods, with mean biases closer to zero for all other conditions.

There is a strong spatial component to Q_{si} uncertainty. Mountain observations have a larger spread among observed values, reflected in the larger uncertainty assigned to those observations (section 2.4). Additionally, each product produces a different spatial pattern of Q_{si} over the Sierra Nevada. Differences in how each product represents spatial patterns of Q_{si} are most pronounced at higher elevations (Figure 6) and over mountainous basins (Figure 7). The positive biases and negative transmissivity anomalies found during precipitation events (section 3.4.2) suggest that the differences between products over the Sierra Nevada may reflect differences in perceived cloudiness between products.

While we have made efforts to quantify the uncertainty in Q_{si} over this study domain, it remains unclear how much an effect a given level of uncertainty has on hydrologically relevant variables. Previous work found that Q_{si} biases of 40 W m^{-2} or more led to a root-mean-square error in modeled SWE of greater than 50 mm, with most of the SWE errors manifested during the spring [*Lapo et al*., 2015b]. Similar work by *Slater et al*. [2013] found that an error of 13 W m^{-2} was equivalent to an error in air temperature of 1°C or an error of 5 days in final snow disappearance in 50% of simulations when reconstructing the snow water equivalent (SWE). From these studies we conclude that the typical level of uncertainty found in this evaluation of estimated Q_{si} is large relative to that required for accurately simulating snow melt. In particular, we call attention to NLDAS, which is a common source of forcing data used in reconstructions of SWE [e.g., *Durand et al*., 2008], since it exhibits large biases, at times exceeding 50 W m^{-2}, over the western crest of the Sierra Nevada during the spring (Figures 3 and 5). This result contradicts other evaluations of NLDAS for use in SWE reconstruction [*Rittger et al*., 2016].

The level of Q_{si} uncertainty also has implications for simulating other land surface properties. For instance, potential evapotranspiration (PET), the evapotranspiration from a saturated surface of grass that completely shades the surface, is a function of the net irradiance.

$$\mathrm{ET_{ref}} = \frac{0.408\Delta(R_n) + \gamma \frac{C_n}{T_{\mathrm{air}}} u\ \mathrm{vpd}}{\Delta + \gamma(1 + C_D u)} \tag{2}$$

Equation (2) and all parameter values (Table 1) are taken from *Irmak et al*. [2012] for PET from a grass surface. To quickly demonstrate the impact of the Q_{si} uncertainty on calculations of PET, we assume meteorological values (Table 1) although the impact on PET remains approximately the same for a range of tested values (not shown). Using the basin-averaged Q_{si} over the Tuolumne Basin in April 2006 from each product, PET varies by 0.8 to 1 mm/d (~15% of the daily total) between PET derived from each product's Q_{si}.

We conclude that the Q_{si} uncertainty found over our example basins in the Sierra Nevada (Figure 7) has substantial implications when simulating the hydrology of the region, a conclusion supported by other studies that evaluated LSMs forced with multiple Q_{si} estimates [*Mizukami et al*., 2014; *Hinkelman et al*., 2015].

4.2. Attributing Q_{si} Uncertainty

The largest biases occurred on days that are classified as darker than normal according to the transmissivity anomaly (section 3.4). We focused on the influence of precipitation, aerosols, and water vapor on the observed biases (Figure 9, section 3.4). Water vapor does not have a relationship with product bias or transmissivity anomaly. The lack of negative transmissivity anomalies due to PWV may occur because of this cloud cover screening in the AERONET data. Water vapor reaches a maximum in the summer, when transmissivity is at its peak. The increase in PWV in the summer is likely offset by the absence in cloud cover. In contrast, AOD does display a relationship with product bias and transmissivity anomaly, which does not display the same seasonality of water vapor.

Screening for precipitation reveals that positive Q_{si} biases and negative transmissivity anomalies occur more commonly on days when precipitation is observed. The occurrence of rain (cloudy conditions) does not completely explain the large biases found in all observations (Figure 9), but it does correspond to negative transmissivity anomalies, which are associated with large mean biases in Q_{si} (Figure 8). Given the high correlation

Table 1. Meteorological Variables Used to Calculate Potential Evapotranspiration (Equation (2))

Variable	Symbol (units)	Value(s)
Air temperature	T_{air} (K)	273.16 to 313.16
Surface temperature	T_{surf} (K)	$T_{air} + 5$
Relative humidity	RH (fraction)	.5
Vapor pressure	e_a (kPa)	$e_a = 6.1078 \exp(17.269388 (T_{air} - 273.16)/(T_{air} - 35.86)/100$
Vapor pressure deficit	VPD (kPa)	$VPD = e_a(T_{air}) - RHe_a(T_{air})$
Albedo	α (fraction)	0.23
Incoming longwave irradiance	Q_{li} (W m^{-2})	235 (MTCLIM over Tuolumne in April 2006)
Outgoing longwave irradiance	Q_{lo} (W m^{-2})	$-(T_{surf}^4)\ 5.67\times10^{-8}$
Incoming solar	Q_{si} (W m^{-2})	
MTCLIM		158
NLDAS		202
SYN		146
WRF		211
Net irradiance	R_n (W m^{-2})	$(1 - \alpha)\ Q_{si} + (Q_{li} + Q_{lo})$

between clouds and precipitation in this study domain, this analysis suggests that cloudy/rainy conditions are when the Q_{si} estimates perform the worst. In particular, rain over California is predominantly driven by atmospheric river events [*Rutz et al.*, 2014], suggesting that either the products or observations have systematic error during periods with synoptically forced clouds. As noted earlier, the spring of 2006, a period during which all products exhibit large, positive biases (Figures 4 and 5), is noteworthy for the number of atmospheric river events. Additionally, biases are spatially distributed across the entire study domain, as demonstrated in Figure 5, suggesting that the meteorological conditions driving the biases should impact the region as a whole. The extensive stratus cloud cover from atmospheric river events (e.g., Figure 2d) is consistent with the spatial structure of the biases. We would expect other factors, such as aerosols, to be constrained by topography and not impact the entire region (e.g., Figure 2c).

The most similar work to this study, *Slater* [2015], analyzed surface observations of Q_{si} over the United States. Both this study and *Slater* [2015] examine how Q_{si} varies over a large region, using lower quality stations instead of spatially isolated but higher quality stations, allowing a systematic evaluation of Q_{si} estimates at scales and in environments largely neglected. Both studies find large differences among products at monthly and seasonal time scales of similar magnitude.

However, there are appreciable differences in our two studies. For instance, *Slater* [2015] concludes that the MTCLIM algorithm, as implemented in the DAYMET product, performs poorly while we find MTCLIM consistently yields Q_{si} within observational uncertainty. While there are substantial differences between the versions of the MTCLIM algorithm used in the two studies, we cannot rule out that the differences in quality control are responsible. Slater, by screening observations to match modeled clear-sky irradiances, effectively removes periods of extensive cloud cover from their results. The result in this study, especially the biases found during periods with precipitation, is a result that Slater could not arrive at. However, the downside to the quality control approach used in this study is the inability to enforce uniformity across observations, both in space and time, which is reflected in the relatively large observational uncertainties that we prescribe. Quality control methodology needs to be carefully considered, as approaches used in either paper may not be appropriate for answering particular questions or applicable to certain data.

The level of uncertainty that both studies demonstrate and the large differences in how we treat surface observations provides motivation for a careful examination of what approaches are appropriate for using these lower quality stations. Due to lower quality instruments used in either study, it is not unreasonable to hypothesize that the biases found could also be the result of instrument error. For instance, the biases we find during negative transmissivity anomalies occur during rainy conditions. One possible explanation is that water could condense on the sensor domes [e.g., *Malek*, 2008], thereby driving observational errors and not product errors. It is clear, though, that these lower quality stations contain useful information, even if the instrument uncertainty is much greater than at the more commonly used high-quality stations. The end conclusion, that Q_{si} is highly uncertainty from the perspective of the land surface, remains unchanged, simply due to the differences found between different methods of estimating Q_{si} (Figures 6 and 7), even if no confidence is placed in the observations.

4.3. Guidance in Using Q_{si} Estimates

Using the best data available and our approach to the second tier surface observations, we believe that MTCLIM v4.2 from the VIC preprocessor, driven by the *Livneh et al*. [2014] data, is the best method for estimating Q_{si} in complex terrain. However, we caution that MTLCIM was only assessed in one region, that there are known, large differences between v4.2 and v4.3 [*Slater*, 2016], that other studies have had mixed results in regards to the MTCLIM algorithm [*Bohn et al*., 2013; *Slater*, 2016], and that the method is sensitive to the forcing data [*Bohn et al*., 2013; *Mizukami et al*., 2014]. MTCLIM reduces its estimates of Q_{si} by 25% on days when precipitation was observed. This precipitation adjustment is a possible explanation for MTCLIM outperforming more sophisticated models.

SYN also performs well relative to observations in the Central Valley, performing within observational uncertainty (Figure 3). However, the influence of spatial scale should be taken into account when selecting a product, for instance, as evident in Figures 5 and 6. SYN has a very coarse spatial resolution and may not be appropriate for environments with steep gradients in cloud cover. *Hakuba et al*. [2013] also noted that the variability of Q_{si} within regions of complex terrain is much higher, making coarse spatial resolution estimates of Q_{si} less representative of local conditions. SYN, as a satellite-derived product, is also subject to the issue of cloud-snow discrimination. That said, both the cloud-snow discrimination and subgrid variability were not found to contribute a significant bias in a previous study [*Hinkelman et al*., 2015].

The evaluation of WRF requires further discussion. WRF exhibits the largest biases, with a strong seasonal cycle. While most uncoupled studies of the land surface do not use WRF irradiances, WRF is commonly employed in studies of land surface processes in coupled settings. Of particular concern is using WRF as a method of regional reanalysis, for instances as implemented in *Rasmussen et al*. [2014]. Rasmussen et al. found large differences between simulated and observed ET at a site within their study domain in the Colorado Headwaters [*Rasmussen et al*., 2014, Figure 8]. The large biases in WRF's Q_{si} during the spring and summer found in this study may partially explain those differences in ET. Others have used WRF coupled to different land surface models to determine which processes are most important for representing the exchange of energy between the land and atmosphere [*Jin and Wen*, 2012]. In this type of study, we suggest that the bias in WRF's Q_{si} will propagate into the land surface component of the model and may bias results. However, the bias in WRF's Q_{si} will strongly depend on the specific configuration [e.g., *Thompson et al*., 2016].

WRF's all-sky Q_{si}, which was found to perform poorly in this study, by default does not include subgrid cloud amount (i.e., generated by the cumulus parameterization) in radiative calculations, an option that was only recently developed [*Thompson et al*., 2016]. In a similar study over Spain, WRF was evaluated to have large, positive biases, especially over a region of complex terrain with meteorology characterized by convective systems. These biases decreased when subgrid cloud amount was included in the radiation scheme [*Ruiz-Arias et al*., 2016]. Others have examined WRF's Q_{si}, but only for clear-sky conditions, attributing errors to factors like aerosols [*Jimenez et al*., 2015; *Zhong et al*., 2016]. While aerosols play a role in the WRF Q_{si} bias found in this study, biases are much larger during cloudy conditions. Based on this study and *Ruiz-Arias et al*. [2016] we suggest that the subgrid cloud be included in the radiation scheme when using WRF to study land surface processes.

We also found that NLDAS performed relatively poorly, specifically yielding large seasonal biases, especially at lower elevations (Figure 3). *Xia et al*. [2016] compared NLDAS radiative fluxes against satellite-derived surface irradiances and found a mean difference of ~10 $W\,m^{-2}$, with larger differences in the summer. While not directly comparable, the result of a positive bias in NDLAS Q_{si} is consistent with this study. *Rittger et al*. [2016] also examined NLDAS irradiances over this region, but with a different set of surface observations. They found that there was no elevation dependence in the median bias of NLDAS' Q_{si}, a result we may expect from this study, given that NLDAS has larger biases at the lower elevation stations than at the higher elevations (Figure 3). However, Rittger et al. did not take into account shading (supporting information, Figure 2) or other quality control issues [*Lapo et al*., 2015a] that exist in their observations.

Even if we neglect surface observations as untrustworthy, uncertainty at higher elevations is substantial. We have shown that this level of uncertainty will likely have a large influence on hydrological modeling. From this result, we suggest that studies with a land surface modeling component use multiple data sets as hypothesis of different forcing data, instead of using one data set assumed to have negligible errors, in order to estimate

the impact of forcing data uncertainty on modeling results. It should be noted that all products evaluated in this study exhibited positive biases. We caution that selecting multiple products, each with a positive bias, may still not adequately sample the uncertainty in Q_{si} for LSM purposes.

5. Conclusions

Studies of land surface processes, especially in complex terrain, often require estimates of meteorological variables used to force land surface models, but these estimates are rarely evaluated within mountainous environments. To understand the Q_{si} uncertainty, we examined different methods of estimating Q_{si} in areas of complex terrain: empirical relationships between proxy variables (MTCLIM), remote sensing (SYN), and downscaled reanalysis (NLDAS and WRF). These products were evaluated over the Central Valley and Sierra Nevada, a region with meteorology strongly impacted by complex topography, using a spatially dense network of surface observations. Large biases, outside the range of estimated observational uncertainty, were found for all products in all subregions examined. Uncertainty, as measured by differences among products, was strongly related to elevation, leading to differences in Q_{si} averaged over mountain basins up to 80 W m^{-2}, although typically less, on the monthly time scale. Finally, errors in estimated Q_{si} were associated with rain (used as a proxy for cloud cover) and were only weakly associated with large AOD and PWV values. We suggest using an ensemble of Q_{si} estimates for forcing LSMs so as to include the range of Q_{si} uncertainty, especially in regions of complex topography.

Acknowledgments

K.E. Lapo was supported by NASA Headquarters under the NASA Earth and Space Science Fellowship Program—grant NNX13AN78H. J.D. Lundquist and M. Hughes acknowledge support from NASA grant NNX15AB29G. Initial funding for this project was provided by NASA grant NNX11AF54G as part of the Science of Terra and Aqua program. The authors wish to applaud both IPM and CIMIS for providing such a well-maintained and described weather database. A huge thank to the UW Mountain Hydrology Research Group for their extensive feedback and comments on this work. All codes used in this study can be found at github.com/klapo/CalRad. Data used in this manuscript are included in the supporting information.

References

Baldocchi, D., and E. Waller (2014), Winter fog is decreasing in the fruit growing region of the Central Valley of California, *Geophys. Res. Lett.*, *41*, 3251–3256, doi:10.1002/2014GL060018.

Bohn, T. J., B. Livneh, J. W. Oyler, S. W. Running, B. Nijssen, and D. P. Lettenmaier (2013), Global evaluation of MTCLIM and related algorithms for forcing of ecological and hydrological models, *Agric. For. Meteorol.*, *176*, 38–49, doi:10.1016/j.agrformet.2013.03.003.

Cline, D. W. (1997), Snow surface energy exchanges and snowmelt at a continental, midlatitude Alpine site, *Water Resour. Res.*, *33*(4), 689–701, doi:10.1029/97WR00026.

Cosgrove, B. A., et al. (2003), Real-time and retrospective forcing in the North American Land Data Assimilation System (NLDAS) project, *J. Geophys. Res.*, *108*(D22), 8842, doi:10.1029/2002JD003118.

Cristea, N. C., S. K. Kampf, and S. J. Burges (2013), Linear models for estimating annual and growing season reference evapotranspiration using averages of weather variables, *Int. J. Climatol.*, *33*(February 2012), 376–387, doi:10.1002/joc.3430.

De Young, R., W. B. Grant, K. Severance, and C. Thornton (2004), Aerosol transport in the California central valley observed by airborne lidar, *Eur. Sp. Agency, (Special Publ. ESA SP)*, *2*(561), 691–694, doi:10.1021/es048740l.

Dettinger, M. D., F. M. Ralph, T. Das, P. J. Neiman, and D. R. Cayan (2011), Atmospheric rivers, floods and the water resources of California, *Water*, *3*(2), 445–478, doi:10.3390/w3020445.

Doelling, D. R., N. G. Loeb, D. F. Keyes, M. L. Nordeen, D. Morstad, C. Nguyen, B. A. Wielicki, D. F. Young, and M. Sun (2013), Geostationary enhanced temporal interpolation for CERES flux products, *J. Atmos. Oceanic Technol.*, *30*(6), 1072–1090, doi:10.1175/JTECH-D-12-00136.1.

Dudhia, J. (1989), Numerical study of convection observed during the winter monsoon experiment using a mesoscale two-dimensional model, *J. Atmos. Sci.*, *46*(20), 3077–3107, doi:10.1175/1520-0469(1989)046<3077:NSOCOD>2.0.CO;2.

Durand, M., N. P. Molotch, and S. A. Margulis (2008), A Bayesian approach to snow water equivalent reconstruction, *J. Geophys. Res.*, *113*, D20117, doi:10.1029/2008JD009894.

Feld, S. I., N. C. Cristea, and J. D. Lundquist (2013), Representing atmospheric moisture content along mountain slopes: Examination using distributed sensors in the Sierra Nevada, California, *Water Resour. Res.*, *49*, 4424–4441, doi:10.1002/wrcr.20318.

Finkelstein, P. L., and L. E. Truppi (1991), Spatial-distribution of precipitation seasonality in the United States, *J. Clim.*, *4*(4), 373–385, doi:10.1175/1520-0442(1991)004<0373:sdopsi>2.0.co;2.

Fu, Q., and K. N. Liou (1993), Parameterization of the radiative properties of cirrus clouds, *J. Atmos. Sci.*, *50*(13), 2008–2025.

Gong, L., C. Y. Xu, D. Chen, S. Halldin, and Y. D. Chen (2006), Sensitivity of the Penman-Monteith reference evapotranspiration to key climatic variables in the Changjiang (Yangtze River) basin, *J. Hydrol.*, *329*(3–4), 620–629, doi:10.1016/j.jhydrol.2006.03.027.

Grubišić, V., and B. J. Billings (2008), Climatology of the Sierra Nevada mountain-wave events, *Mon. Weather Rev.*, *136*(2), 757–768, doi:10.1175/2007MWR1902.1.

Guan, B., N. P. Molotch, D. E. Waliser, E. J. Fetzer, and P. J. Neiman (2010), Extreme snowfall events linked to atmospheric rivers and surface air temperature via satellite measurements, *Geophys. Res. Lett.*, *37*, L20401, doi:10.1029/2010GL044696.

Hakuba, M. Z., D. Folini, A. Sanchez-Lorenzo, and M. Wild (2013), Spatial representativeness of ground-based solar radiation measurements, *J. Geophys. Res. Atmos.*, *118*, 8585–8597, doi:10.1002/jgrd.50673.

Hinkelman, L. M., T. P. Ackerman, and R. T. Marchand (1999), An evaluation of NCEP Eta model predictions of surface energy budget and cloud properties by comparison with measured ARM data, *J. Geophys. Res.*, *104*, 19,535–19,549, doi:10.1029/1999JD900120.

Hinkelman, L. M., K. E. Lapo, N. C. Cristea, and J. D. Lundquist (2015), Using CERES SYN surface irradiance data as forcing for snowmelt simulation in complex terrain, *J. Hydrometeorol.*, doi:10.1175/JHM-D-14-0179.1.

Hinkelman, L., T. Zhang, and P. Stackhouse (2012), *Comparisons of Satellite-Estimated Radiative Fluxes Reaching the Surface to Ground Observations*, edited by E. Raschke, S. Kinne, and P. W. Stackhouse, World Climate Research Programme.

Holben, B. N., et al. (1998), AERONET—A federated instrument network and data archive for aerosol characterization, *Remote Sens. Environ.*, *66*(1), 1–16, doi:10.1016/S0034-4257(98)00031-5.

Hong, S.-Y., Y. Noh, and J. Dudhia (2006), A new vertical diffusion package with an explicit treatment of entrainment processes, *Mon. Weather Rev.*, *134*(9), 2318–2341, doi:10.1175/MWR3199.1.

Hughes, M., P. J. Neiman, E. Sukovich, and M. Ralph (2012), Representation of the Sierra Barrier Jet in 11 years of a high-resolution dynamical reanalysis downscaling compared with long-term wind profiler observations, *J. Geophys. Res.*, *117*, D18116, doi:10.1029/2012JD017869.

Irmak, S., I. Kabenge, K. E. Skaggs, and D. Mutiibwa (2012), Trend and magnitude of changes in climate variables and reference evapotranspiration over 116-yr period in the Platte River Basin, central Nebraska-USA, *J. Hydrol.*, *420–421*, 228–244, doi:10.1016/j.jhydrol.2011.12.006.

Iziomon, M. G., H. Mayer, W. Wicke, and A. Matzarakis (2001), Radiation balance over low-lying and mountainous areas in south-west Germany, *Theor. Appl. Climatol.*, *68*(3–4), 219–231, doi:10.1007/s007040170047.

Jimenez, P. A., J. P. Hacker, J. Dudhia, S. Ellen Haupt, J. A. Ruiz-Arias, C. A. Gueymard, G. Thompson, T. Eidhammer, and A. Deng (2015), WRF-Solar: An augmented NWP model for solar power prediction. Model description and clear sky assessment, *Bull. Am. Meteorol. Soc.*, 151029072131009, doi:10.1175/BAMS-D-14-00279.1.

Jin, J., and L. Wen (2012), Evaluation of snowmelt simulation in the Weather Research and Forecasting model, *J. Geophys. Res.*, *117*, D10110, doi:10.1029/2011JD016980.

Kain, J. S. (2004), The Kain–Fritsch convective parameterization: An update, *J. Appl. Meteorol.*, *43*(1), 170–181, doi:10.1175/1520-0450(2004)043<0170:TKCPAU>2.0.CO;2.

Kato, S., F. G. Rose, and T. P. Charlock (2005), Computation of domain-averaged irradiance using satellite-derived cloud properties, *J. Atmos. Oceanic Technol.*, *22*(2), 146–164, doi:10.1175/JTECH-1694.1.

Langlois, A., J. Kohn, A. Royer, P. Cliche, L. Brucker, G. Picard, M. Fily, C. Derksen, and J. M. Willemet (2009), Simulation of snow water equivalent (SWE) using thermodynamic snow models in Québec, Canada, *J. Hydrometeorol.*, *10*(6), 1447–1463, doi:10.1175/2009JHM1154.1.

Lapo, K. E., L. M. Hinkelman, C. C. Landry, A. K. Massman, and J. D. Lundquist (2015a), A simple algorithm for identifying periods of snow accumulation on a radiometer, *Water Resour. Res.*, *51*, 7820–7828, doi:10.1002/2015WR017590.

Lapo, K. E., L. M. Hinkelman, M. S. Raleigh, and J. D. Lundquist (2015b), Impact of errors in the downwelling irradiances on simulations of snow water equivalent, snow surface temperature, and the snow energy balance, *Water Resour. Res.*, *51*, 5772–5790, doi:10.1002/2014WR016259.

Lewis, J., R. De Young, R. Ferrare, and D. Allen Chu (2010), Comparison of summer and winter California central valley aerosol distributions from lidar and MODIS measurements, *Atmos. Environ.*, *44*(35), 4510–4520, doi:10.1016/j.atmosenv.2010.07.006.

Liang, X., D. P. Lettenmaier, E. F. Wood, and J. Burges (1994), A simple hydrologically based model of land surface water and energy fluxes for general circulation models, *J. Geophys. Res.*, *99*(D7), 14,415–14,428, doi:10.1029/94JD00483.

Livneh, B., E. A. Rosenberg, C. Lin, B. Nijssen, V. Mishra, K. M. Andreadis, E. P. Maurer, and D. P. Lettenmaier (2014), A long-term hydrologically based dataset of land surface fluxes and states for the conterminous United States: Update and extensions, *J. Clim.*, *27*(1), 477–486, doi:10.1175/JCLI-D-13-00697.1.

Long, C. N., and Y. Shi (2008), An automated quality assessment and control algorithm for surface radiation measurements, *Open Atmos. Sci. J.*, *2*(1), 23–37, doi:10.2174/1874282300802010023.

Lundquist, J. D., and D. R. Cayan (2007), Surface temperature patterns in complex terrain: Daily variations and long-term change in the central Sierra Nevada, California, *J. Geophys. Res.*, *112*, D11124, doi:10.1029/2006JD007561.

Lundquist, J. D., N. E. Wayand, A. K. Massman, M. P. Clark, F. Lott, and N. C. Cristea (2015), Diagnosis of insidious data disasters, *Water Resour. Res.*, *51*, 2498–2514, doi:10.1002/2014WR016585.

Luo, L. (2003), Validation of the North American Land Data Assimilation System (NLDAS) retrospective forcing over the southern Great Plains, *J. Geophys. Res.*, *108*(D22), 8843, doi:10.1029/2002JD003246.

Malek, E. (2008), The daily and annual effects of dew, frost, and snow on a non-ventilated net radiometer, *Atmos. Res.*, *89*(3), 243–251, doi:10.1016/j.atmosres.2008.02.006.

Marty, C., R. Philipona, C. Frohlich, and A. Ohmura (2002), Altitude dependence of surface radiation fluxes and cloud forcing in the Alps: Results from the alpine surface radiation budget network, *Theor. Appl. Climatol.*, *72*, 137–155.

Mazurkiewicz, A. B., D. G. Callery, and J. J. McDonnell (2008), Assessing the controls of the snow energy balance and water available for runoff in a rain-on-snow environment, *J. Hydrol.*, *354*(1–4), 1–14, doi:10.1016/j.jhydrol.2007.12.027.

McMeeking, G. R., et al. (2006), Smoke-impacted regional haze in California during the summer of 2002, *Agric. For. Meteorol.*, *137*(1–2), 25–42, doi:10.1016/j.agrformet.2006.01.011.

Ménard, C. B., J. Ikonen, K. Rautiainen, M. Aurela, A. N. Arslan, and J. Pulliainen (2015), Effects of meteorological and ancillary data, temporal averaging and evaluation methods on model performance and uncertainty in a land surface model, *J. Hydrometeorol.*, *16*, 2559–2576, doi:10.1175/JHM-D-15-0013.1.

Mesinger, F., et al. (2006), North American Regional Reanalysis, *Bull. Am. Meteorol. Soc.*, *87*(3), 343–360, doi:10.1175/BAMS-87-3-343.

Mizukami, N., M. P. Clark, A. G. Slater, L. D. Brekke, M. M. Elsner, J. R. Arnold, and S. Gangopadhyay (2014), Hydrologic implications of different large-scale meteorological model forcing datasets in mountainous regions, *J. Hydrometeorol.*, *15*(1), 474–488, doi:10.1175/JHM-D-13-036.1.

Mlawer, E. J., S. J. Taubman, P. D. Brown, M. J. Iacono, and S. A. Clough (1997), Radiative transfer for inhomogeneous atmospheres: RRTM, a validated correlated-k model for the longwave, *J. Geophys. Res.*, *102*(D14), 16,663–16,682, doi:10.1029/97JD00237.

Morrison, H., G. Thompson, and V. Tatarskii (2009), Impact of cloud microphysics on the development of trailing stratiform precipitation in a simulated squall line: Comparison of one- and two-moment schemes, *Mon. Weather Rev.*, *137*(3), 991–1007, doi:10.1175/2008MWR2556.1.

Olyphant, G. A. (1984), Insolation topoclimates and potential ablation in Alpine snow accumulation basins' Front Range, Colorado Cirque Glacier, *Water Resour. Res.*, *20*(4), 491–498, doi:10.1029/WR020i004p00491.

Painter, T. H., et al. (2015), The Airborne Snow Observatory: Scanning lidar and imaging spectrometer fusion for mapping snow water equivalent and snow albedo, *Remote Sens. Environ.*, doi:10.1016/j.rse.2016.06.018.

Philipona, R. (2002), Underestimation of solar global and diffuse radiation measured at Earth's surface, *J. Geophys. Res.*, *107*(D22), 4654, doi:10.1029/2002JD002396.

Pinker, R. T., D. Tarpley, I. Laszlo, K. Mitchell, and P. Houser (2003), Surface radiation budgets in support of the GEWEX Continental-Scale International Project (GCIP) and the GEWEX Americas Prediction Project (GAPP), including the North American Land Data Assimilation System (NLDAS) project, *J. Geophys. Res.*, *108*(D22), 8844, doi:10.1029/2002JD003301.

Raleigh, M. S., J. D. Lundquist, and M. P. Clark (2015), Exploring the impact of forcing error characteristics on physically based snow simulations within a global sensitivity analysis framework, *Hydrol. Earth Syst. Sci.*, *19*(7), 3153–3179, doi:10.5194/hess-19-3153-2015.

Ralph, F. M., et al. (2013), The emergence of weather-related test beds linking research and forecasting operations, *Bull. Am. Meteorol. Soc.*, *94*(8), 1187–1211, doi:10.1175/BAMS-D-12-00080.1.

Raschke, E., S. Kinne, and P. W. Stackhouse (2012), GEWEX Radiative Flux Assessment (RFA) Volume 1: Assessment.
Rasmussen, R., et al. (2014), Climate change impacts on the water balance of the Colorado Headwaters: High-resolution regional climate model simulations, *J. Hydrometeorol.*, *15*(3), 1091–1116, doi:10.1175/JHM-D-13-0118.1.
Rittger, K., E. H. Bair, A. Kahl, and J. Dozier (2016), Spatial estimates of snow water equivalent from reconstruction, *Adv. Water Resour.*, *94*, 345–363, doi:10.1016/j.advwatres.2016.05.015.
Ruiz-Arias, J. A., C. Arbizu-Barrena, F. J. Santos-Alamillos, J. Tovar-Pescador, and D. Pozo-Vázquez (2016), Assessing the surface solar radiation budget in the WRF model: A spatiotemporal analysis of the bias and its causes, *Mon. Weather Rev.*, *144*(2), 703–711, doi:10.1175/MWR-D-15-0262.1.
Rutan, D. A., S. Kato, D. R. Doelling, F. G. Rose, L. T. Nguyen, T. E. Caldwell, and N. G. Loeb (2015), CERES synoptic product: Methodology and validation of surface radiant flux, *J. Atmos. Oceanic Technol.*, *32*(6), 1121–1143, doi:10.1175/JTECH-D-14-00165.1.
Rutter, N., et al. (2009), Evaluation of forest snow processes models (SnowMIP2), *J. Geophys. Res.*, *114*, D06111, doi:10.1029/2008JD011063.
Rutz, J. J., W. J. Steenburgh, and F. M. Ralph (2014), Climatological characteristics of atmospheric rivers and their inland penetration over the western United States, *Mon. Weather Rev.*, *142*, 905–921, doi:10.1175/MWR-D-13-00168.1.
Schroeder, T. A., R. Hember, N. C. Coops, and S. Liang (2009), Validation of solar radiation surfaces from MODIS and reanalysis data over topographically complex terrain, *J. Appl. Meteorol. Climatol.*, *48*(12), 2441–2458, doi:10.1175/2009JAMC2152.1.
Sengupta, M., P. Gotseff, and T. Stoffel (2012), Evaluation of photodiode and thermopile pyranometers for photovoltaic applications, in *27th European Photovoltaic Solar Energy Conference and Exhibition*, pp. 3705–3708.
Shi, X., M. Sturm, G. E. Liston, R. E. Jordan, and D. P. Lettenmaier (2009), SnowSTAR2002 transect reconstruction using a multilayered energy and mass balance snow model, *J. Hydrometeorol.*, *10*(5), 1151–1167, doi:10.1175/2009JHM1098.1.
Simpson, J. J., M. D. Dettinger, F. Gehrke, T. J. McIntire, and G. L. Hufford (2004), Hydrologic scales, cloud variability, remote sensing, and models: Implications for forecasting snowmelt and streamflow, *Weather Forecasting*, *19*(2), 251–276.
Skamarock, W. C., J. B. Klemp, J. Dudhi, D. O. Gill, D. M. Barker, M. G. Duda, X.-Y. Huang, W. Wang, and J. G. Powers (2008), A description of the Advanced Research WRF version 3, *NCAR Tech. Note*, (June), 113, doi:10.5065/D6DZ069T.
Slater, A. G. (2015), Surface solar radiation in North America: A comparison of observations, reanalyses, satellite and derived products, *J. Hydrometeorol.*, *17*, 401–420, doi:10.1175/JHM-D-15-0087.1.
Slater, A. G. (2016), Surface solar radiation in North America: A comparison of observations, reanalyses, satellite, and derived products*, *J. Hydrometeorol.*, *17*(1), 401–420, doi:10.1175/JHM-D-15-0087.1.
Slater, A. G., A. P. Barrett, M. P. Clark, J. D. Lundquist, and M. Raleigh (2013), Uncertainty in seasonal snow reconstruction: Relative impacts of model forcing and image availability, *Adv. Water Resour.*, *55*, 165–177.
Tang, W., K. Yang, J. He, and J. Qin (2010), Quality control and estimation of global solar radiation in China, *Sol. Energy*, *84*(3), 466–475, doi:10.1016/j.solener.2010.01.006.
Tewari, M., F. Chen, W. Wang, J. Dudhia, M. A. LeMone, K. Mitchell, M. Ek, G. Gayno, J. Wegiel, and R. H. Cuenca (2004), Implementation and verification of the unified Noah land surface model in the WRF model, in *20th Conference on Weather Analysis and Forecasting/16th Conference on Numerical Weather Prediction*, pp. 11–15.
Thompson, G., M. Tewari, K. Ikeda, S. Tessendorf, C. Weeks, J. Otkin, and F. Kong (2016), Explicitly-coupled cloud physics and radiation parameterizations and subsequent evaluation in WRF high-resolution convective forecasts, *Atmos. Res.*, *168*, 92–104, doi:10.1016/j.atmosres.2015.09.005.
Thornton, P. E., and H. Hasenauer (2000), Simultaneous estimation of daily solar radiation and humidity from observed temperature and precipitation: An application over complex terrain in Austria, *Agric. For.*, *104*, 255–271.
Thornton, P. E., and S. W. Running (1999), An improved algorithm for estimating incident daily solar radiation from measurements of temperature, humidity, and precipitation, *Agric. For. Meteorol.*, *93*, 211–228.
Underwood, S. J., G. P. Ellrod, and A. L. Kuhnert (2004), A multiple-case analysis of nocturnal radiation-fog development in the Central Valley of California utilizing the GOES nighttime fog product, *J. Appl. Meteorol.*, *43*(2), 297–311, doi:10.1175/1520-0450(2004)043<0297:AMAONR>2.0.CO;2.
Vignola, F., L. Vuilleumier, and J. Gröbner (2014), Effects of changing spectral radiation distribution on the performance of photodiode pyranometers, in *Intersol North American*, American Solar Energy Society, San Francisco, Calif.
Viviroli, D., H. H. Du, B. Messerli, M. Meybeck, and R. Weingartner (2007), Mountains of the world, water towers for humanity: Typology, mapping, and global significance, *Water Resour. Res.*, *43*, W07447, doi:10.1029/2006WR005653.
Wang, K., J. Augustine, and R. E. Dickinson (2012), Critical assessment of surface incident solar radiation observations collected by SURFRAD, USCRN and AmeriFlux networks from 1995 to 2011, *J. Geophys. Res.*, *117*, D23105, doi:10.1029/2012JD017945.
Wielicki, B. A., B. R. Barkstrom, B. A. Baum, T. P. Charlock, and R. N. Green (1998), Clouds and the Earth's Radiant Energy System (CERES): Algorithm overview, *IEEE Trans. Geosci. Remote Sens.*, *36*(4), 1127–1141, doi:10.1029/2005WR003976.
World Meteorological Organization (2008), Measurement of radiation, in *Guide to Meteorological Instruments and Methods of Observation*, pp. I.7-1–1.7-42, World Meteorological Organization, Geneva, Switzerland.
Xia, Y., Z.-L. Yang, P. L. Stoffa, and K. Sen Mrinal (2005), Using different hydrological variables to assess the impacts of atmospheric forcing errors on optimization and uncertainty analysis of the CHASM surface model at a cold catchment, *J. Geophys. Res.*, *110*, D01101, doi:10.1029/2004JD005130.
Xia, Y., B. A. Cosgrove, K. Mitchell, C. D. Peters-Lidard, M. B. Ek, S. Kumar, D. Mocko, and H. Wei (2016), Basin-scale assessment of the land surface energy budget in the National Centers for Environmental Prediction operational and research NLDAS-2 systems, *J. Geophys. Res. Atmos.*, *121*, 196–220, doi:10.1002/2015JD023889.
Yang, K., J. He, W. Tang, J. Qin, and C. C. K. Cheng (2010), On downward shortwave and longwave radiations over high altitude regions: Observation and modeling in the Tibetan Plateau, *Agric. For. Meteorol.*, *150*(1), 38–46, doi:10.1016/j.agrformet.2009.08.004.
Ying, Q., and M. Kleeman (2009), Regional contributions to airborne particulate matter in central California during a severe pollution episode, *Atmos. Environ.*, *43*(6), 1218–1228, doi:10.1016/j.atmosenv.2008.11.019.
Zhang, Q., and C. Anastasio (2001), Chemistry of fog waters in California's Central Valley—Part 3: Concentrations and speciation of organic and inorganic nitrogen, *Atmos. Environ.*, *35*(32), 5629–5643, doi:10.1016/S1352-2310(01)00337-5.
Zhang, T., P. W. Stackhouse, S. K. Gupta, S. J. Cox, J. Colleen Mikovitz, and L. M. Hinkelman (2012), The validation of the GEWEX SRB surface shortwave flux data products using BSRN measurements: A systematic quality control, production and application approach, *J. Quant. Spectros. Radiat. Transfer*, *122*, 127–140, doi:10.1016/j.jqsrt.2012.10.004.
Zhong, X., J. A. Ruiz-Arias, and J. Kleissl (2016), Dissecting surface clear sky irradiance bias in numerical weather prediction: Application and corrections to the New Goddard Shortwave Scheme, *Sol. Energy*, *132*, 103–113, doi:10.1016/j.solener.2016.03.009.